Efficient propagation-inside-layer expansion algorithm for solving the scattering from three-dimensional nested homogeneous dielectric bodies with arbitrary shape

Sami Bellez,[1,*] Christophe Bourlier,[1] and Gildas Kubické[2]

[1]*IETR (Institut d'Électronique et de Télécommunications de Rennes) Laboratory, LUNAM Université, Université de Nantes, Nantes, France*

[2]*DGA/DT/MI (Direction Générale de l'Armement-Direction Technique-Maîtrise de l'Information), CGN1 Division, Bruz, France*

**Corresponding author: sami.bellez@univ-nantes.fr*

Received September 16, 2014; revised November 12, 2014; accepted November 26, 2014; posted January 12, 2015 (Doc. ID 223281); published February 6, 2015

This paper deals with the evaluation of electromagnetic scattering from a three-dimensional structure consisting of two nested homogeneous dielectric bodies with arbitrary shape. The scattering problem is formulated in terms of a set of Poggio–Miller–Chang–Harrington–Wu integral equations that are afterwards converted into a system of linear equations (impedance matrix equation) by applying the Galerkin method of moments (MoM) with Rao–Wilton–Glisson basis functions. The MoM matrix equation is then solved by deploying the iterative propagation-inside-layer expansion (PILE) method in order to obtain the unknown surface current densities, which are thereafter used to handle the radar cross-section (RCS) patterns. Some numerical results for various structures including canonical geometries are presented and compared with those of the FEKO software in order to validate the PILE-based approach as well as to show its efficiency to analyze the full-polarized RCS patterns.

OCIS codes: (290.5825) Scattering theory; (290.5855) Scattering, polarization; (290.4210) Multiple scattering; (000.3860) Mathematical methods in physics; (050.1755) Computational electromagnetic methods.

http://dx.doi.org/10.1364/JOSAA.32.000392

1. INTRODUCTION

Recent years have seen increasing interest in efficient and accurate solution of electromagnetic (EM) scattering from dielectric layered bodies with arbitrarily shape chiefly because of the importance of the nondestructive testing (NDT) of composite materials as well as the stealth characteristic for the military system design. In particular, there is great interest in studying the reflective and absorptive properties of targets in order to achieve a reduction of the radar cross section (RCS) over a wide range of frequencies at specific scattering directions. However, most of the earlier techniques have been utilized to solve two-dimensional (2D) problems [1,2], bodies of revolution [3,4], three-dimensional (3D) homogeneous bodies [5–8], and 3D perfectly conducting bodies [9–16] coated with a lossy material [17–19].

Integral equation solvers [20,21] based on the method of moments (MoM) [22] are often deployed because they offer an "exact" description of the interaction of a radar signal with an arbitrarily shaped structure while exact analytical solutions are only available for canonical geometries such as spheres and spheroids [23]. The surface integral equation (SIE) approach is often preferred for homogeneous and piecewise homogeneous structures since it limits the discretization of the unknowns to the surface of the structure and the discontinuous interfaces between different materials. The volume integral equation (VIE) approach appears to be more advantageous for a structure with arbitrary inhomogeneity.

The SIE approach, widely used in the frequency domain, is based on the fact that the field inside any homogeneous body can be represented in terms of the equivalent surface current densities on its boundary surface using either the equivalence principle or the vector Green's theorem [20]. For a structure consisting of a finite number of homogeneous bodies, a piecewise representation of the EM field inside the structure leads to a system of SIEs over the body boundary surfaces. The integral equation system must then be solved to find the unknown surface current densities, which can subsequently be used to represent the field everywhere.

The Poggio–Miller–Chang–Harrington–Wu (PMCHW) formulation [24,25] is generally employed as it eliminates the interior resonance problem and it normally yields to a better conditioned matrix equation as compared to electric field integral equation (EFIE) formulation [26] or magnetic field integral equation (MFIE) formulation [26]. The combined field integral equation (CFIE) formulation [8,27] can also be applied with suitable expansion and testing functions to avoid the interior resonance problem.

In this work, we propose a generalization of the PMCHW formulation in order to treat a structure composed of two homogeneous dielectric scatterers where only one is illuminated by the EM incident plane wave. The PMCHW integral

equations are discretized by using the Galerkin MoM [28] with Rao–Wilton–Glisson (RWG) basis functions defined on triangular patches [10], which converts them to a system of N linear equations (a matrix equation) with N being the number of unknown quantities. The matrix equation can be solved using a direct or an iterative solver. Both solvers are limited in their application to $\mathcal{O}(N^2)$ memory space to store the MoM matrix elements. Furthermore, the complexity of a direct solver is $\mathcal{O}(N^3)$, while for an iterative solver it is $\mathcal{O}(N^2)$ per iteration. These requirements have prevented the use of the conventional MoM to solve electrically large problems involving a large number of unknowns. In the case of a structure consisting of two nested homogeneous objects, the propagation-inside-layer expansion (PILE) method [29], based on a domain decomposition, is a good candidate for improving the computational cost in terms of central processing unit (CPU) time and storage requirements. Indeed, it avoids the direct solution of the whole MoM matrix equation by using the partitioned inverse matrix formulas and an iterative scheme. Besides, the PILE method offers a straightforward physical interpretation of the scattering process. It was initially developed to study 2D scattering problems such as the scattering from a stack of two one-dimensional interfaces separating homogeneous media [29], the scattering from a buried object under a randomly rough surface [30], and the scattering from coated spheres and spheroids [2,31]. There are two steps in the PILE method procedure: the first step is dedicated to handling the initial current densities on the illuminated surface, and the second one, repeated in an iterative process, to account for the current densities due to the coupling interactions between scatterers. In both steps, acceleration algorithms can be applied and will be the subject of our future work.

In this paper, we address the application of the PILE method for solving the MoM matrix equation of a 3D structure consisting of two nested homogeneous scatterers with arbitrary shape. It should be noted that the PILE method has never been tested on a such configuration. The paper is organized as follows. Section 2 presents the EM formulation of the problem from the surface integral representations of the EM field to the adopted PMCHW surface integral formulation. The special case of a perfectly conducting interior scatterer is also treated. Section 3 describes the Galerkin MoM discretization procedure. Section 4 presents the resolution of the MoM matrix equation using the PILE method. Section 5 deals with memory and computational complexities of the PILE-based solver. Section 6 shows the numerical results, and finally Section 7 gives concluding remarks and prospects.

2. PROBLEM GEOMETRY AND EM FORMULATION

A. Problem Geometry

Let us consider the scattering of an EM plane wave by a 3D structure embedded in an isotropic homogeneous background medium $\mathcal{D}_1$, which is usually free space, with dielectric parameters (ϵ_1, μ_1). The problem geometry is illustrated in Fig. 1. The structure consists of two nested arbitrarily shaped homogeneous dielectric objects. The interior object (ϵ_3, μ_3), occupying the region $\mathcal{D}_3$ bounded by the surface S_{23}, is confined within the domain $\mathcal{D}_2$ of the exterior object (ϵ_2, μ_2) bounded by the surfaces S_{12} and S_{23}. The unit normal vector to the surface S_{12} pointing into the domain D_1 is denoted $\hat{\mathbf{n}}_{\mathcal{D}_1}^{S_{12}}$, while the unit vector $\hat{\mathbf{n}}_{\mathcal{D}_2}^{S_{12}}$ is that pointing into the domain $\mathcal{D}_2$. Similarly, $\hat{\mathbf{n}}_{\mathcal{D}_2}^{S_{23}}$ and $\hat{\mathbf{n}}_{\mathcal{D}_3}^{S_{23}}$ are the unit normal vectors to the surface S_{23} pointing, respectively, into the domains $\mathcal{D}_2$ and $\mathcal{D}_3$.

B. EM Field Surface Integral Representations

The analysis of EM scattering from two nested homogeneous bodies using the surface equivalence principle involves three equivalent problems (representing the original physical problem) that need to be combined to take into account the solution in the different domains. The field inside any domain $\mathcal{D}_i$ can be represented as the sum of an exciting field and a scattering field generated by the unknown equivalent surface current densities on the domain boundary surface. From these considerations, an integral representation of the fields inside each domain can be derived. In the case of the $\mathcal{D}_1$ equivalent problem, the total EM field $(\mathbf{E}_1, \mathbf{H}_1)$ in $\mathcal{D}_1$ is equal to the sum of the incident EM field $(\mathbf{E}_1^{\text{inc}}, \mathbf{H}_1^{\text{inc}})$ and the scattering EM field generated by the equivalent sources on the interface S_{12} $(\mathbf{J}_{\mathcal{D}_1}^{S_{12}}, \mathbf{M}_{\mathcal{D}_1}^{S_{12}})$ for any observation point $\mathbf{r} \in \mathcal{D}_1$. The total EM field is zero; otherwise $(\mathbf{r} \notin \mathcal{D}_1)$. This implies that the equivalent sources produce an EM field that exactly cancels the incident EM field (extinction theorem):

$$\left.\begin{array}{l} \forall\ \mathbf{r} \in \mathcal{D}_1, \mathbf{E}_1(\mathbf{r}) \\ \forall\ \mathbf{r} \notin \mathcal{D}_1, \mathbf{0} \end{array}\right\} = \mathbf{E}_1^{\text{inc}}(\mathbf{r}) + \eta_1 \mathcal{L}_1(\mathbf{J}_{\mathcal{D}_1}^{S_{12}})(\mathbf{r}) - \mathcal{K}_1(\mathbf{M}_{\mathcal{D}_1}^{S_{12}})(\mathbf{r}), \tag{1a}$$

$$\left.\begin{array}{l} \forall\ \mathbf{r} \in \mathcal{D}_1, \mathbf{H}_1(\mathbf{r}) \\ \forall\ \mathbf{r} \notin \mathcal{D}_1, \mathbf{0} \end{array}\right\} = \mathbf{H}_1^{\text{inc}}(\mathbf{r}) + \frac{1}{\eta_1} \mathcal{L}_1(\mathbf{M}_{\mathcal{D}_1}^{S_{12}})(\mathbf{r}) + \mathcal{K}_1(\mathbf{J}_{\mathcal{D}_1}^{S_{12}})(\mathbf{r}), \tag{1b}$$

where $\mathcal{L}_1$ and $\mathcal{K}_1$ are integral operators whose expressions are given by Eq. (6).

For the $\mathcal{D}_2$ equivalent problem, the space is homogenized with the dielectric parameters ϵ_2 and μ_2. For any observation point $\mathbf{r} \in \mathcal{D}_2$, the total EM field $(\mathbf{E}_2, \mathbf{H}_2)$ is equal to the sum of the exciting EM field generated by the equivalent sources on the boundary surface S_{12} and the scattering EM field generated by the equivalent sources on the boundary surface S_{23} of the scatterer occupying the domain $\mathcal{D}_3$. The total EM field is null; otherwise

$$\left.\begin{array}{l} \forall\ \mathbf{r} \in \mathcal{D}_2, \mathbf{E}_2(\mathbf{r}) \\ \forall\ \mathbf{r} \notin \mathcal{D}_2, \mathbf{0} \end{array}\right\} = \eta_2 \mathcal{L}_2(\mathbf{J}_{\mathcal{D}_2}^{S_{12}})(\mathbf{r}) + \eta_2 \mathcal{L}_2(\mathbf{J}_{\mathcal{D}_2}^{S_{23}})(\mathbf{r}) - \mathcal{K}_2(\mathbf{M}_{\mathcal{D}_2}^{S_{12}})(\mathbf{r}) - \mathcal{K}_2(\mathbf{M}_{\mathcal{D}_2}^{S_{23}})(\mathbf{r}), \tag{2a}$$

$$\left.\begin{array}{l} \forall\ \mathbf{r} \in \mathcal{D}_2, \mathbf{H}_2(\mathbf{r}) \\ \forall\ \mathbf{r} \notin \mathcal{D}_2, \mathbf{0} \end{array}\right\} = \frac{1}{\eta_2} \mathcal{L}_2(\mathbf{M}_{\mathcal{D}_2}^{S_{12}})(\mathbf{r}) + \frac{1}{\eta_2} \mathcal{L}_2(\mathbf{M}_{\mathcal{D}_2}^{S_{23}})(\mathbf{r}) + \mathcal{K}_2(\mathbf{J}_{\mathcal{D}_2}^{S_{12}})(\mathbf{r}) + \mathcal{K}_2(\mathbf{J}_{\mathcal{D}_2}^{S_{23}})(\mathbf{r}). \tag{2b}$$

In the case of the $\mathcal{D}_3$ equivalent problem and for any observation point $\mathbf{r} \in \mathcal{D}_3$, the total EM field $(\mathbf{E}_3, \mathbf{H}_3)$ is only equal to the EM field generated by the equivalent sources on the boundary surface S_{23} because there is no excitation by an EM field inside the observation domain. In addition, the total EM field is null for any observation point $\mathbf{r} \notin \mathcal{D}_3$:

$$\left.\begin{array}{c}\forall\ \mathbf{r}\in\mathcal{D}_3, \mathbf{E}_3(\mathbf{r})\\ \forall\ \mathbf{r}\notin\mathcal{D}_3, \mathbf{0}\end{array}\right\} = \eta_3\mathcal{L}_3(\mathbf{J}^{S_{23}}_{\mathcal{D}_3})(\mathbf{r}) - \mathcal{K}_3(\mathbf{M}^{S_{23}}_{\mathcal{D}_3})(\mathbf{r}), \tag{3a}$$

$$\left.\begin{array}{c}\forall\ \mathbf{r}\in\mathcal{D}_3, \mathbf{H}_3(\mathbf{r})\\ \forall\ \mathbf{r}\notin\mathcal{D}_3, \mathbf{0}\end{array}\right\} = \frac{1}{\eta_3}\mathcal{L}_3(\mathbf{M}^{S_{23}}_{\mathcal{D}_3})(\mathbf{r}) + \mathcal{K}_3(\mathbf{J}^{S_{23}}_{\mathcal{D}_3})(\mathbf{r}), \tag{3b}$$

where η_i ($i = 1$, 2, or 3) is the complex impedance of the domain $\mathcal{D}_i$ defined as

$$\eta_i = \sqrt{\frac{\mu_i}{\epsilon_i}} \tag{4}$$

and

$$\epsilon_i = \epsilon_0\left(\epsilon_i^r - j\frac{\sigma_i}{\omega\epsilon_0}\right), \tag{5a}$$

$$\mu_i = \mu_0, \tag{5b}$$

where ϵ_i^r and σ_i are, respectively, the relative permittivity and the conductivity of the domain $\mathcal{D}_i$; ϵ_0 and μ_0 are, respectively, the vacuum permittivity and permeability; and ω is the angular frequency. The operators $\mathcal{L}_i$ and $\mathcal{K}_i$ are defined as

$$\mathcal{L}_i(\mathbf{X})(\mathbf{r}) = -jk_i\int_S G_i(\mathbf{r},\mathbf{r}')\mathbf{X}(\mathbf{r}')\mathrm{d}S' + \frac{j}{k_i}\nabla'\int_S G_i(\mathbf{r},\mathbf{r}')\nabla'\cdot\mathbf{X}(\mathbf{r}')\mathrm{d}S', \tag{6a}$$

$$\mathcal{K}_i(\mathbf{X})(\mathbf{r}) = \int_S \mathbf{X}(\mathbf{r}')\times\nabla' G_i(\mathbf{r},\mathbf{r}')\mathrm{d}S', \tag{6b}$$

where k_i and $G_i(\mathbf{r},\mathbf{r}')$ are, respectively, the wavenumber and the scalar Green's function associated with the domain $\mathcal{D}_i$; S is the integration surface representing S_{12} or S_{23}; and finally $\mathbf{X}$ is the input variable of the operators representing surface current densities $\mathbf{J}^{S_{12}}_{\mathcal{D}_1}$, $\mathbf{J}^{S_{12}}_{\mathcal{D}_2}$, $\mathbf{J}^{S_{23}}_{\mathcal{D}_2}$, $\mathbf{J}^{S_{23}}_{\mathcal{D}_3}$, $\mathbf{M}^{S_{12}}_{\mathcal{D}_1}$, $\mathbf{M}^{S_{12}}_{\mathcal{D}_2}$, $\mathbf{M}^{S_{23}}_{\mathcal{D}_2}$, or $\mathbf{M}^{S_{23}}_{\mathcal{D}_3}$. The expression of the scalar Green's function is given by

$$G_i(\mathbf{r},\mathbf{r}') = \frac{e^{-jk_iR}}{4\pi R}, \tag{7}$$

where $R = \sqrt{(x-x')^2+(y-y')^2+(z-z')^2}$ is the distance between the observation point $\mathbf{r}$ and the source point $\mathbf{r}'$.

C. Surface Integral Equation Formulations

By piecewise representation of the EM field inside the homogeneous domains ($\mathcal{D}_1$, $\mathcal{D}_2$, and $\mathcal{D}_3$), the original physical problem is transformed into a system of eight SIEs over the boundary surfaces S_{12} and S_{23} of the domains. The equation to calculate the electric field is known as the EFIE, and there are four such equations: $\mathrm{EFIE}^{S^{\mathcal{D}_1}_{12}}$, $\mathrm{EFIE}^{S^{\mathcal{D}_2}_{12}}$, $\mathrm{EFIE}^{S^{\mathcal{D}_2}_{23}}$, and $\mathrm{EFIE}^{S^{\mathcal{D}_3}_{23}}$. The surfaces $S^{\mathcal{D}_1}_{12}$ and $S^{\mathcal{D}_2}_{12}$ are respectively selected to be slightly above (in $\mathcal{D}_1$) and below (in $\mathcal{D}_2$) the surface S_{12}, while the surfaces $S^{\mathcal{D}_2}_{23}$ and $S^{\mathcal{D}_3}_{23}$ are respectively selected to be slightly above (in $\mathcal{D}_2$) and below (in $\mathcal{D}_3$) the surface S_{23}. The equation to calculate the magnetic field is known as the MFIE, and there are also four such equations: $\mathrm{MFIE}^{S^{\mathcal{D}_1}_{12}}$, $\mathrm{MFIE}^{S^{\mathcal{D}_2}_{12}}$, $\mathrm{MFIE}^{S^{\mathcal{D}_2}_{23}}$, and $\mathrm{MFIE}^{S^{\mathcal{D}_3}_{23}}$. Since there are eight equations and four unknowns, it is possible to develop a number of different formulations for solving the surface current densities. For example, one can select the four EFIEs or the four MFIEs to form a system of equations for a solution of $\mathbf{J}^{S_{12}}$, $\mathbf{M}^{S_{12}}$, $\mathbf{J}^{S_{23}}$, and $\mathbf{M}^{S_{23}}$. Unfortunately, both the EFIE and the MFIE formulations suffer from the spurious interior resonance problem, and their weighted linear combination, known as the CFIE, is usually adopted as a remedy. Another possible way of obtaining a unique solution at an internal resonant frequency is to use the so-called PMCHW formulation, which is very often employed in the analysis of 3D dielectric bodies by combining the EFIEs and MFIEs on both sides of the body boundary interface as

$$-[\mathbf{E}_1^{\mathrm{inc}}(\mathbf{r})]_{\tan} = [(\eta_1\mathcal{L}_1+\eta_2\mathcal{L}_2)(\mathbf{J}^{S_{12}})(\mathbf{r}) - (\mathcal{K}_1+\mathcal{K}_2)(\mathbf{M}^{S_{12}})(\mathbf{r}) - \eta_2\mathcal{L}_2(\mathbf{J}^{S_{23}})(\mathbf{r}) + \mathcal{K}_2(\mathbf{M}^{S_{23}})(\mathbf{r})]_{\tan}, \tag{8a}$$

$$-[\mathbf{H}_1^{\mathrm{inc}}(\mathbf{r})]_{\tan} = \left[(\mathcal{K}_1+\mathcal{K}_2)(\mathbf{J}^{S_{12}})(\mathbf{r}) + \left(\frac{1}{\eta_1}\mathcal{L}_1+\frac{1}{\eta_2}\mathcal{L}_2\right)(\mathbf{M}^{S_{12}})(\mathbf{r}) - \mathcal{K}_2(\mathbf{J}^{S_{23}})(\mathbf{r}) \quad -\frac{1}{\eta_2}\mathcal{L}_2(\mathbf{M}^{S_{23}})(\mathbf{r})\right]_{\tan}, \tag{8b}$$

$$\mathbf{0} = [-\eta_2\mathcal{L}_2(\mathbf{J}^{S_{12}})(\mathbf{r}) + \mathcal{K}_2(\mathbf{M}^{S_{12}})(\mathbf{r}) + (\eta_2\mathcal{L}_2+\eta_3\mathcal{L}_3)(\mathbf{J}^{S_{23}})(\mathbf{r}) - (\mathcal{K}_2+\mathcal{K}_3)(\mathbf{M}^{S_{23}})(\mathbf{r})]_{\tan}, \tag{8c}$$

$$\mathbf{0} = \left[-\mathcal{K}_2(\mathbf{J}^{S_{12}})(\mathbf{r}) - \frac{1}{\eta_2}\mathcal{L}_2(\mathbf{M}^{S_{12}})(\mathbf{r}) + (\mathcal{K}_2+\mathcal{K}_3)(\mathbf{J}^{S_{23}})(\mathbf{r}) + \left(\frac{1}{\eta_2}\mathcal{L}_2+\frac{1}{\eta_3}\mathcal{L}_3\right)(\mathbf{M}^{S_{23}})(\mathbf{r})\right]_{\tan}. \tag{8d}$$

It is important to underline that the integral inside the operator $\mathcal{K}_i(\mathbf{X})$ (with $i = 1$, 2, or 3 and $\mathbf{X} = \mathbf{J}^{S_{12}}$, $\mathbf{M}^{S_{12}}$, $\mathbf{J}^{S_{23}}$, or $\mathbf{M}^{S_{23}}$) must be understood in the Cauchy principal value (CPV) sense, as the other part is in the $\mathbf{X}/2$ term.

Let us now consider the special case in which the domain $\mathcal{D}_3$ is occupied by a perfectly conducting body ($\mathbf{M}^{S_{23}}$ is null). In this case, the expressions in the equation can be simplified by removing the integral operators acting on the magnetic current density $\mathbf{M}^{S_{23}}(\mathcal{L}_i(\mathbf{M}^{S_{23}}), \mathcal{K}_i(\mathbf{M}^{S_{23}}))$ and those with dielectric parameters of the domain $\mathcal{D}_3(\mathcal{L}_3, \mathcal{K}_3)$. After these simplifications, we need only three integral equations to determine the unknown quantities since the magnetic current density on the surface S_{23} is null. In our case, we use the EFIE formulation for the metallic surface and the PMCHW formulation for the dielectric interface:

$$-[\mathbf{E}_1^{\mathrm{inc}}(\mathbf{r})]_{\tan} = [(\eta_1\mathcal{L}_1+\eta_2\mathcal{L}_2)(\mathbf{J}^{S_{12}})(\mathbf{r}) - (\mathcal{K}_1+\mathcal{K}_2)(\mathbf{M}^{S_{12}})(\mathbf{r}) - \eta_2\mathcal{L}_2(\mathbf{J}^{S_{23}})(\mathbf{r})]_{\tan}, \tag{9a}$$

$$-[\mathbf{H}_1^{\mathrm{inc}}(\mathbf{r})]_{\tan} = \left[(\mathcal{K}_1+\mathcal{K}_2)(\mathbf{J}^{S_{12}})(\mathbf{r}) + \left(\frac{1}{\eta_1}\mathcal{L}_1+\frac{1}{\eta_2}\mathcal{L}_2\right)(\mathbf{M}^{S_{12}})(\mathbf{r}) - \mathcal{K}_2(\mathbf{J}^{S_{23}})(\mathbf{r})\right]_{\tan}, \tag{9b}$$

$$\mathbf{0} = [-\eta_2\mathcal{L}_2(\mathbf{J}^{S_{12}})(\mathbf{r}) + \mathcal{K}_2(\mathbf{M}^{S_{12}})(\mathbf{r}) + \eta_2\mathcal{L}_2(\mathbf{J}^{S_{23}})(\mathbf{r})]_{\tan}. \quad (9c)$$

However, if the structure includes a closed metallic surface, the EFIE [Eq. (9c)] is not sufficient for removing the interior resonances. In such a case, Eq. (9c) is replaced by the CFIE (10) to avoid this problem:

$$\begin{aligned}\mathbf{0} = \alpha[&-\eta_2\mathcal{L}_2(\mathbf{J}^{S_{12}})(\mathbf{r}) + \eta_2\mathcal{L}_2(\mathbf{J}^{S_{23}})(\mathbf{r})\\ &+ \mathcal{K}_2(\mathbf{M}^{S_{12}})(\mathbf{r})]_{\tan} + (1-\alpha)\eta_2\hat{\mathbf{n}}^{S_{23}}(\mathbf{r})\\ &\times\left[-\mathcal{K}_2(\mathbf{J}^{S_{12}})(\mathbf{r}) - \frac{1}{\eta_2}\mathcal{L}_2(\mathbf{M}^{S_{12}})(\mathbf{r})\right.\\ &\left.+\mathcal{K}_2(\mathbf{J}^{S_{23}})(\mathbf{r}) + \hat{\mathbf{n}}^{S_{23}}(\mathbf{r})\times\frac{\mathbf{J}^{S_{23}}(\mathbf{r})}{2}\right], \quad (10)\end{aligned}$$

where the constant α is chosen so that the spurious solution is eliminated. Typically a good choice of α is $0.2 \le \alpha \le 0.4$.

The solution of the integral equation formulations (8)–(10) yields to the electric and magnetic surface current densities. These current densities can be used to evaluate the fields scattered by a given structure, at any point $\mathbf{r} \in \mathcal{D}_1$, by using the following expressions:

$$\mathbf{E}_1^{\text{sca}}(\mathbf{r}) = \eta_1\mathcal{L}_1(\mathbf{J}^{S_{12}})(\mathbf{r}) - \mathcal{K}_1(\mathbf{M}^{S_{12}})(\mathbf{r}), \quad \forall\ \mathbf{r} \in \mathcal{D}_1, \quad (11a)$$

$$\mathbf{H}_1^{\text{sca}}(\mathbf{r}) = \frac{1}{\eta_1}\mathcal{L}_1(\mathbf{M}^{S_{12}})(\mathbf{r}) + \mathcal{K}_1(\mathbf{J}^{S_{12}})(\mathbf{r}), \quad \forall\ \mathbf{r} \in \mathcal{D}_1. \quad (11b)$$

In the far-field zone, the integral operators $\mathcal{L}_1$ and $\mathcal{K}_1$ can be simplified to $\mathcal{L}_1^{\text{FF}}$ and $\mathcal{K}_1^{\text{FF}}$ as

$$\mathcal{L}_1^{\text{FF}}(\mathbf{X}) = j\frac{k_1}{4\pi}\frac{e^{-jk_1r}}{r}\hat{\mathbf{k}}^s\times\hat{\mathbf{k}}^s\times\int_{S_{12}}\mathbf{X}(\mathbf{r}')e^{jk_1\mathbf{r}'\cdot\hat{\mathbf{k}}^s}\mathrm{d}S'_{12}, \quad (12a)$$

$$\mathcal{K}_1^{\text{FF}}(\mathbf{X}) = -j\frac{k_1}{4\pi}\frac{e^{-jk_1r}}{r}\hat{\mathbf{k}}^s\times\int_{S_{12}}\mathbf{X}(\mathbf{r}')e^{jk_1\mathbf{r}'\cdot\hat{\mathbf{k}}^s}\mathrm{d}S'_{12}, \quad (12b)$$

where $\hat{\mathbf{k}}^s$ is the scattering direction and r is the distance from the origin to the receiver position.

The scattered fields are afterward needed in the computation of the RCS, which is defined as

$$\text{RCS}_{pq} = 4\pi r^2\frac{|\mathbf{E}_1^{\text{sca}}(\mathbf{r})\cdot\hat{\mathbf{q}}^s|^2}{|\mathbf{E}_1^{\text{inc}}(\mathbf{r})\cdot\hat{\mathbf{p}}^i|^2} = 4\pi r^2\frac{|\mathbf{H}_1^{\text{sca}}(\mathbf{r})\cdot\hat{\mathbf{q}}^s|^2}{|\mathbf{H}_1^{\text{inc}}(\mathbf{r})\cdot\hat{\mathbf{p}}^i|^2}, \quad (13)$$

where $\hat{\mathbf{p}}^i$ and $\hat{\mathbf{q}}^s$, respectively, are the incidence and scattering polarization unit vectors.

3. DISCRETIZATION OF THE SURFACE INTEGRAL EQUATIONS

The PMCHW formulation for the scattering from two nested arbitrarily shaped dielectric homogeneous objects is posed in terms of unknown current densities. In order to convert the continuous SIEs to a matrix equation, we use the most versatile numerical technique referred to as the MoM. The first step in the MoM procedure is to discretize the object boundary surfaces into a set of patches much smaller than the wavelength. Weighted basis functions acting as expansion functions for the unknown current densities are then associated with these patches. The most common basis functions for a triangular patch were introduced by Rao *et al.* [10] and are thus called RWG basis functions. For a pair of adjacent triangles T_n^+ and T_n^- sharing a common edge of length ℓ_n, these are defined by

$$\mathbf{f}_n(\mathbf{r}) = \begin{cases}\frac{\ell_n}{2A_n^+}\boldsymbol{\rho}_n^+(\mathbf{r}), & \text{if } \mathbf{r}\in T_n^+\\ \frac{\ell_n}{2A_n^-}\boldsymbol{\rho}_n^-(\mathbf{r}), & \text{if } \mathbf{r}\in T_n^-\\ 0, & \text{otherwise}\end{cases}, \quad (14)$$

where $A_n^\pm$ denotes the area of the triangle $T_n^\pm$, and $\boldsymbol{\rho}_n^\pm$ is a tangential vector expressed as

$$\boldsymbol{\rho}_n^\pm = \pm(\mathbf{r}_n^\pm - \mathbf{r}), \qquad \mathbf{r}\in T_n^\pm \quad (15)$$

with $\mathbf{r}_n^\pm$ the free vertex of the triangle $T_n^\pm$.

In order to solve the integral equations (8) with the MoM, the electric and magnetic currents on the surface S_{12} are expanded in terms of a known set of $N^{S_{12}}$ basis functions, $\mathbf{f}_j(\mathbf{r})$, as

$$\mathbf{J}^{S_{12}}(\mathbf{r}) \approx \sum_{j=1}^{N^{S_{12}}} a_j^{S_{12}}\mathbf{f}_j(\mathbf{r}), \quad \forall\ \mathbf{r}\in S_{12}, \quad (16a)$$

$$\mathbf{M}^{S_{12}}(\mathbf{r}) \approx \sum_{j=1}^{N^{S_{12}}} b_j^{S_{12}}\mathbf{f}_j(\mathbf{r}), \quad \forall\ \mathbf{r}\in S_{12}, \quad (16b)$$

and the electric and magnetic currents on the surface S_{23} are expanded in terms of a known set of $N^{S_{23}}$ basis functions, $\mathbf{f}_n(\mathbf{r})$, as

$$\mathbf{J}^{S_{23}}(\mathbf{r}) \approx \sum_{n=1}^{N^{S_{23}}} a_n^{S_{23}}\mathbf{f}_n(\mathbf{r}), \quad \forall\ \mathbf{r}\in S_{23}, \quad (17a)$$

$$\mathbf{M}^{S_{23}}(\mathbf{r}) \approx \sum_{n=1}^{N^{S_{23}}} b_n^{S_{23}}\mathbf{f}_n(\mathbf{r}), \quad \forall\ \mathbf{r}\in S_{23}, \quad (17b)$$

where $a_j^{S_{12}}$ and $b_j^{S_{12}}$ are, respectively, the unknown weights of the expansions for the electric $\mathbf{J}^{S_{12}}(\mathbf{r})$ and magnetic $\mathbf{M}^{S_{12}}(\mathbf{r})$ currents and $a_n^{S_{23}}$ and $b_n^{S_{23}}$ are the unknown weights of the expansions for the electric $\mathbf{J}^{S_{23}}(\mathbf{r})$ and magnetic $\mathbf{M}^{S_{23}}(\mathbf{r})$ currents, respectively. In this case, the same basis functions have been used to expand the electric and magnetic currents on both surfaces. Next, the test functions are chosen equal to the basis functions (Galerkin's method) yielding to a system of $(N = 2N^{S_{12}} + 2N^{S_{23}})$ linear equations that are cast in a matrix equation composed of an impedance matrix $\mathbf{Z}$, an unknown vector $\boldsymbol{\alpha}$, and a right-hand side vector $\mathbf{V}$:

$$\begin{bmatrix}\mathbf{Z}_{S_{12}S_{12}} & \mathbf{Z}_{S_{12}S_{23}}\\ \mathbf{Z}_{S_{23}S_{12}} & \mathbf{Z}_{S_{23}S_{23}}\end{bmatrix}\begin{bmatrix}\boldsymbol{\alpha}_{S_{12}}\\ \boldsymbol{\alpha}_{S_{23}}\end{bmatrix} = \begin{bmatrix}\mathbf{V}_{S_{12}}\\ \mathbf{V}_{S_{23}}\end{bmatrix}$$

$$\begin{bmatrix}\mathbf{Z}^{\mathbf{EJ}}_{S_{12}S_{12}} & \mathbf{Z}^{\mathbf{EM}}_{S_{12}S_{12}} & \mathbf{Z}^{\mathbf{EJ}}_{S_{12}S_{23}} & \mathbf{Z}^{\mathbf{EM}}_{S_{12}S_{23}}\\ \mathbf{Z}^{\mathbf{HJ}}_{S_{12}S_{12}} & \mathbf{Z}^{\mathbf{HM}}_{S_{12}S_{12}} & \mathbf{Z}^{\mathbf{HJ}}_{S_{12}S_{23}} & \mathbf{Z}^{\mathbf{HM}}_{S_{12}S_{23}}\\ \mathbf{Z}^{\mathbf{EJ}}_{S_{23}S_{12}} & \mathbf{Z}^{\mathbf{EM}}_{S_{23}S_{12}} & \mathbf{Z}^{\mathbf{EJ}}_{S_{23}S_{23}} & \mathbf{Z}^{\mathbf{EM}}_{S_{23}S_{23}}\\ \mathbf{Z}^{\mathbf{HJ}}_{S_{23}S_{12}} & \mathbf{Z}^{\mathbf{HM}}_{S_{23}S_{12}} & \mathbf{Z}^{\mathbf{HJ}}_{S_{23}S_{23}} & \mathbf{Z}^{\mathbf{MM}}_{S_{23}S_{23}}\end{bmatrix}\begin{bmatrix}\boldsymbol{\alpha}^{\mathbf{J}}_{S_{12}}\\ \boldsymbol{\alpha}^{\mathbf{M}}_{S_{12}}\\ \boldsymbol{\alpha}^{\mathbf{J}}_{S_{23}}\\ \boldsymbol{\alpha}^{\mathbf{M}}_{S_{23}}\end{bmatrix} = \begin{bmatrix}\mathbf{V}^{\mathbf{E}}_{S_{12}}\\ \mathbf{V}^{\mathbf{H}}_{S_{12}}\\ \mathbf{V}^{\mathbf{E}}_{S_{23}}\\ \mathbf{V}^{\mathbf{H}}_{S_{23}}\end{bmatrix}. \quad (18)$$

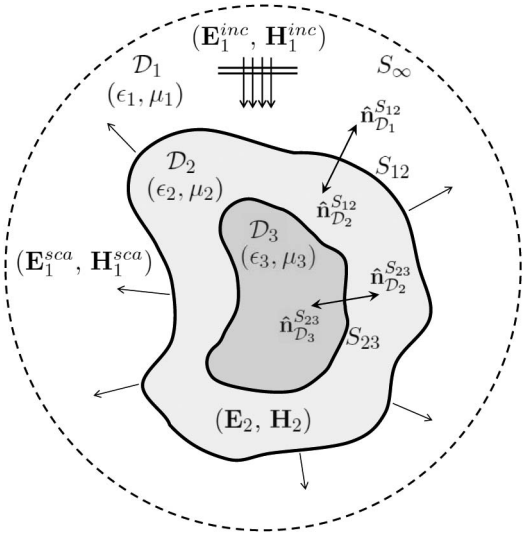

Fig. 1. Original physical problem: geometry of a structure ($\mathcal{D}_2 \cup \mathcal{D}_3$) consisting of two nested homogeneous dielectric scatterers embedded in an isotropic medium ($\mathcal{D}_1$). The structure is illuminated by an incident EM plane wave ($\mathbf{E}_1^{\text{inc}}$, $\mathbf{H}_1^{\text{inc}}$), which is generated by impressed sources in the background medium $\mathcal{D}_1$.

The impedance matrix $\mathbf{Z}$ contains four submatrices: the submatrices $\mathbf{Z}_{S_{12}S_{12}}$ and $\mathbf{Z}_{S_{12}S_{12}}$ are self-impedance matrices describing the local interactions between basis and testing functions on the dielectric surfaces S_{12} and S_{23}, respectively. The submatrices $\mathbf{Z}_{S_{12}S_{23}}$ and $\mathbf{Z}_{S_{23}S_{12}}$ are mutual-impedance matrices. The mutual-impedance matrix $\mathbf{Z}_{S_{12}S_{23}}$ (or $\mathbf{Z}_{S_{23}S_{12}}$) characterizes the coupling interactions between the basis functions of the surface S_{23} (or S_{12}) and the testing functions of the surface S_{12} (or S_{23}). Each submatrix is composed of four submatrices describing the interactions between basis and testing functions associated with the electric and magnetic current densities. The right-hand side vector (excitation vector) is also composed of four subvectors: the vectors $\mathbf{V}_{S_{12}}^{\mathbf{E}}$ and $\mathbf{V}_{S_{12}}^{\mathbf{H}}$ represent, respectively, the electric and magnetic incident fields on the surface S_{12}. Meanwhile, the vectors $\mathbf{V}_{S_{23}}^{\mathbf{E}}$ and $\mathbf{V}_{S_{23}}^{\mathbf{H}}$ represent the electric and magnetic incident fields on the surface S_{23}, respectively. The elements of these vectors are equal to zero because the surface S_{23} is not illuminated by the incident wave [see Fig. 2(a)].

4. SOLVING THE MATRIX INTEGRAL EQUATION

The discretization of the integral equations with the MoM has led to a system of N linear equations that must be solved to obtain the surface current densities, where $N = 2N^{S_{12}} + 2N^{S_{23}}$. The direct solution of the resulting MoM matrix equation via LU decomposition is extremely time consuming or impossible (in terms of computational complexity $\mathcal{O}(N^3)$ and storage $\mathcal{O}(N^2)$) when the problem geometry becomes large compared to the wavelength (N becomes large). Therefore, a possible candidate is the iterative PILE solver [29]. Because the computation of the scattered fields only requires explicit knowledge of the current densities on the surface S_{12}, the MoM matrix equation can be rearranged as

$$\boldsymbol{\alpha}_{S_{12}} = (\mathbf{I} - \mathbf{M}_{S_{12}}^{c})^{-1}\mathbf{Z}_{S_{12}S_{12}}^{-1}\mathbf{V}_{S_{12}}, \tag{19}$$

where $\mathbf{I}$ is the identity matrix and $\mathbf{M}_{S_{12}}^{c}$ is the characteristic matrix of the structure defined as

$$\mathbf{M}_{S_{12}}^{c} = \mathbf{Z}_{S_{12}S_{12}}^{-1}\mathbf{Z}_{S_{12}S_{23}}\mathbf{Z}_{S_{23}S_{23}}^{-1}\mathbf{Z}_{S_{23}S_{12}}. \tag{20}$$

The Taylor expansion of the inverse of the matrix $(\mathbf{I} - \mathbf{M}_{S_{12}}^{c})$ is given by

$$(\mathbf{I} - \mathbf{M}_{S_{12}}^{c})^{-1} = \sum_{p=0}^{p=\infty} (\mathbf{M}_{S_{12}}^{c})^{p}. \tag{21}$$

By putting Eq. (21) into Eq. (19), we obtain the final equation:

$$\boldsymbol{\alpha}_{S_{12}}^{(P_{\text{PILE}})} = \sum_{p=0}^{p=P_{\text{PILE}}} (\mathbf{M}_{S_{12}}^{c})^{p}\mathbf{Z}_{S_{12}S_{12}}^{-1}\mathbf{V}_{S_{12}}. \tag{22}$$

The series is truncated at order $p = P_{\text{PILE}}$ according to the following convergence criterion:

$$\frac{\|\boldsymbol{\alpha}_{S_{12}}^{(p)} - \boldsymbol{\alpha}_{S_{12}}^{(p-1)}\|_2}{\|\boldsymbol{\alpha}_{S_{12}}^{(p)}\|_2} < \Delta_{S_{12}}. \tag{23}$$

In this paper an error of $\Delta_{S_{12}} = 1\%$ is used for all numerical simulations. The convergence order P_{PILE} of the PILE method

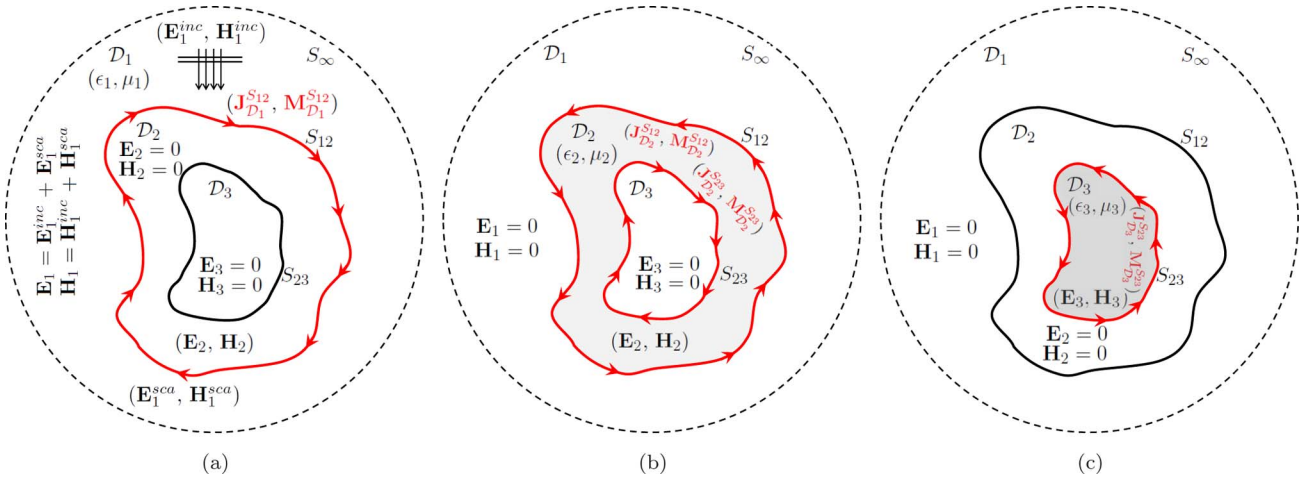

Fig. 2. Equivalent problems representing the original physical problem. (a) $\mathcal{D}_1$ equivalent problem, (b) $\mathcal{D}_2$ equivalent problem, and (c) $\mathcal{D}_3$ equivalent problem.

has a physical meaning because it corresponds to the number of back and forths of the scattering fields between the surfaces S_{12} and S_{23}. The scattering process is as follows: (1) the incident wave $\mathbf{V}_{S12}$ illuminates the surface S_{12} of the structure. (2) The matrix-vector product $\mathbf{Z}_{S_{12}S_{12}}^{-1}\mathbf{V}_{S12}$ gives the zeroth-order electric and magnetic current densities $\boldsymbol{\alpha}_{S_{12}}^{(0)}$ on the surface S_{12}. These current densities are the same as those obtained when the structure only contains the exterior object bounded by the surface S_{12}. (3) The first-order electric and magnetic current densities are then $\boldsymbol{\alpha}_{S_{12}}^{(1)} = \boldsymbol{\alpha}_{S_{12}}^{(0)} + \mathbf{M}_{S_{12}}^{c}\boldsymbol{\alpha}_{S_{12}}^{(0)}$. The matrix-vector product $\mathbf{M}_{S_{12}}^{c}\boldsymbol{\alpha}_{S_{12}}^{(0)}$ gives the current densities caused by the coupling effect between the surfaces in a back-and-forth manner. The matrix-vector product $\mathbf{Z}_{S_{23}S_{12}}\boldsymbol{\alpha}_{S_{12}}^{(0)} = \mathbf{W}_{S_{23}}^{(0)}$ represents the fields scattered from the surface S_{12} exciting the surface S_{23}. $\mathbf{Z}_{S_{23}S_{23}}^{-1}\mathbf{W}_{S_{23}}^{(0)} = \boldsymbol{\alpha}_{S_{23}}^{(0)}$ computes the current densities $\boldsymbol{\alpha}_{S_{23}}^{(0)}$ on the surface S_{23}. $\mathbf{Z}_{S_{12}S_{23}}\boldsymbol{\alpha}_{S_{23}}^{(0)} = \mathbf{W}_{S_{12}}^{(0)}$ represents the fields scattered from the surface S_{23} exciting the surface S_{12}. Finally, $\mathbf{Z}_{S_{12}S_{12}}^{-1}\mathbf{W}_{S_{12}}^{(0)} = \mathbf{M}_{S_{12}}^{c}\boldsymbol{\alpha}_{S_{12}}^{(0)}$ gives the current densities induced by the fields scattered by the surface S_{23}. The sum $\boldsymbol{\alpha}_{S_{12}}^{(1)} = \boldsymbol{\alpha}_{S_{12}}^{(0)} + \mathbf{M}_{S_{12}}^{c}\boldsymbol{\alpha}_{S_{12}}^{(0)}$ updates the current densities on the surface S_{12}. (4) The process is repeated until the norm error criterion is satisfied.

5. MEMORY AND COMPUTATIONAL COMPLEXITIES OF THE PILE-BASED SOLVER

The computational cost of the PILE method depends on how the method is programmed. There are two ways involving a trade-off between computational and memory complexities. The first one is related to the following computations:

- Initialization step

✓ Compute the initial electric and magnetic current densities on S_{12} based on a direct LU solver: $\mathcal{O}(M_{S_{12}}^3)$ multiplications and $\mathcal{O}(M_{S_{12}}^2)$ memory space to store the elements of the self-impedance matrix of the surface S_{12}, where $M_{S_{12}} = 2\,N^{S_{12}}$ is the number of unknowns on S_{12}.

- Repeated (P_{PILE} times) steps until a convergence is reached

✓ Compute the EM field scattered from S_{12} to S_{23} using a matrix-vector product: $\mathcal{O}(M_{S_{23}}M_{S_{12}})$ multiplications and $\mathcal{O}(M_{S_{23}}M_{S_{12}})$ memory space to store the elements of the mutual-impedance matrix characterizing the scattering from S_{12} to S_{23}.
✓ Compute the electric and magnetic current densities on S_{23} based on a direct LU solver: $\mathcal{O}(M_{S_{23}}^3)$ multiplications and $\mathcal{O}(M_{S_{23}}^2)$ memory space to store the elements of the self-impedance matrix of the surface S_{23}, where $M_{S_{23}} = 2\,N^{S_{23}}$ is the number of unknowns on S_{23}.
✓ Compute the EM field scattered from S_{23} to S_{12} using a matrix-vector product: $\mathcal{O}(M_{S_{12}}M_{S_{23}})$ multiplications and $\mathcal{O}(M_{S_{12}}M_{S_{23}})$ memory space to store the elements of the mutual-impedance matrix characterizing the scattering from S_{23} to S_{12}.
✓ Compute high-order electric and magnetic current densities on S_{12} based on a direct LU solver: $\mathcal{O}(M_{S_{12}}^3)$ multiplications and $\mathcal{O}(M_{S_{12}}^2)$ memory space to store the elements of the self-impedance matrix of the surface S_{12}.

According to these computations, the operational count of the PILE-based solver is $\mathcal{O}(M_{S_{12}}^3 + P_{\mathrm{PILE}}(M_{S_{12}}^3 + M_{S_{23}}^3 + 2M_{S_{12}}M_{S_{23}}))$, while that of the direct solver is $\mathcal{O}((M_{S_{12}} + M_{S_{23}})^3)$. Consequently, the computational complexity increases rapidly with the convergence order P_{PILE}. As a result, for few iterations, this approach does not allow us to have better performance in terms of CPU time (without applying any fast solver to invert the self-impedance matrices) in comparison with the direct LU solution of the whole MoM matrix equation. However, there is another way to program the PILE method involving a much lower computational complexity than the first way. So, it seems more advantageous to start by computing and storing the LU decomposition of both self-impedance matrices in the initialization step as follows.

- Initialization step

✓ Compute and store the **L** and **U** decomposition triangular matrices of the self-impedance matrices and compute the initial electric and magnetic current densities on S_{12}: $\mathcal{O}(M_{S_{12}}^3 + M_{S_{23}}^3 + M_{S_{12}}^2)$ operations.

- Repeated (P_{PILE} times) steps until a convergence is reached

✓ Compute the EM field scattered field from S_{12} to S_{23} using a matrix-vector product: $\mathcal{O}(M_{S_{23}}M_{S_{12}})$ multiplications.
✓ Compute the electric and magnetic current densities on S_{23} based on a direct LU solver (only matrix-vector product): $\mathcal{O}(M_{S_{23}}^2)$ multiplications.
✓ Compute the EM field scattered from S_{23} to S_{12} using a matrix-vector product: $\mathcal{O}(M_{S_{12}}M_{S_{23}})$ multiplications.
✓ Compute the high-order electric and magnetic current densities on S_{12} based on a direct LU solver (only matrix-vector product): $\mathcal{O}(M_{S_{12}}^2)$ multiplications.

The complexity of the PILE method is then reduced to $\mathcal{O}(M_{S_{12}}^3 + M_{S_{12}}^2 + M_{S_{23}}^3 + P_{\mathrm{PILE}}(M_{S_{12}}^2 + M_{S_{23}}^2 + 2M_{S_{12}}M_{S_{23}}))$ because, inside the iterative process, the inversions of the self-impedance matrices are reduced to only matrix-vector products. In summary, the PILE method can be programmed in two ways depending on the computer storage capacity, and it can be classified as fast when $\mathcal{O}((M_{S_{23}} + M_{S_{12}})^2)$ memory space is available.

6. SIMULATION RESULTS

In this section, some numerical simulations are presented to validate the implementation procedure and to demonstrate the accuracy of the PILE-based method. Our study considers three structure geometries that are illuminated by an EM plane wave at the frequency $f = 300$ MHz ($\lambda_1 = 1$ m) in the incidence direction $\hat{\mathbf{k}}_i(\theta_i = 0°, \phi_i = 0°)$. It is vertically and then horizontally polarized. The scattered field is evaluated in the far-field zone in the scattering direction $\hat{\mathbf{k}}_s(\theta_s, \phi_s)$ defined by θ_s varying from –90° to 90° with an angular step of 2° and $\phi_s = \phi_i$. The first structure $\mathcal{S}_1$ consists of two concentric homogeneous dielectric spheres. The interior sphere characterized by the relative permittivity $\epsilon_{\mathrm{in}}^r = 2 - j8$ and the radius $r_{\mathrm{in}} = 0.5\lambda_1$ is embedded in an exterior sphere having the relative permittivity $\epsilon_{\mathrm{ex}}^r = 2 - j0.1$ and the radius $r_{\mathrm{ex}} = \lambda_1$. The interior and exterior spheres are respectively discretized into 5376 and 10,780 triangular patches, which results in 24,234 edges and 48,468 unknowns. The second structure $\mathcal{S}_2$ is composed of two concentric dielectric tilted

cylinders. The interior cylinder of relative permittivity $\epsilon_{\text{in}}^r = 2 - j12$, radius $r_{\text{in}} = 0.5\lambda_1$, and length $h_{\text{in}} = 2\lambda_1$ is embedded in an exterior cylinder characterized by the relative permittivity $\epsilon_{\text{ex}}^r = 2 - j0.1$, the radius $r_{\text{ex}} = 0.3\lambda_1$, and the length $h_{\text{ex}} = 3\lambda_1$. The interior and exterior cylinders are respectively discretized into 4826 and 8876 triangular patches leading to 20,553 edges and 41,106 unknowns. The third structure $\mathcal{S}_3$ consists of a PEC tilted cylinder having the radius $r_{\text{in}} = 0.2\lambda_1$ and the length $h_{\text{in}} = 0.8\lambda_1$ embedded in a dielectric sphere of radius $r_{\text{ex}} = \lambda_1$ characterized by the relative permittivity $\epsilon_{\text{ex}}^r = 2 - j0.1$. The interior cylinder and the exterior sphere are respectively discretized into 1880 and 12,660 triangular patches involving 21,810 edges and 40,800 unknowns. All of the considered cylinders are initially oriented with their axis in the $\hat{\mathbf{z}}$ direction and then are tilted by successively applying a rotation of 45° about the $\hat{\mathbf{x}}$ axis and another rotation of 45° about the $\hat{\mathbf{y}}$ axis, so as to have nonzero cross-polarized levels.

In Fig. 3(a), we present the bistatic RCS of the structure $\mathcal{S}_1$ as well as the phase of the scattered field as a function of the angle θ_s for VV and HH polarizations. The cross-polarization (HV and VH) returns are not plotted for this configuration because they are null due to symmetry reasons. The curves in Fig. 3(a) show good agreement between the FEKO and PILE-based solutions in magnitude and phase for both VV and HH polarization channels. The PILE-based method converges to the FEKO solution after $P_{\text{PILE}} = 4$ iterations with an error of 0.31%. It can also be seen that the PILE-based solution at $p = 3$ gives a satisfactory result with an error of 1.45%. This physically means that there are four back and forths of the scattering fields between the sphere interfaces. We underline that the solution at the order $p = 0$ corresponds to that of the exterior sphere placed in free space in the absence of the interior sphere. Furthermore, we notice a slight difference between the RCS levels in the specular direction $\hat{\mathbf{k}}_s(\theta_s = 0°, \phi_s = 0°)$. This difference is about 0.4 dB for both copolarizations. In addition, due to the symmetry of the structure $\mathcal{S}_1$, the curves are also symmetric about the specular direction.

The cross-polarized RCS values shown in Figs. 4(b) and 4(c) are not null when the incidence and the scattering planes are the same and represent a target symmetry plane.

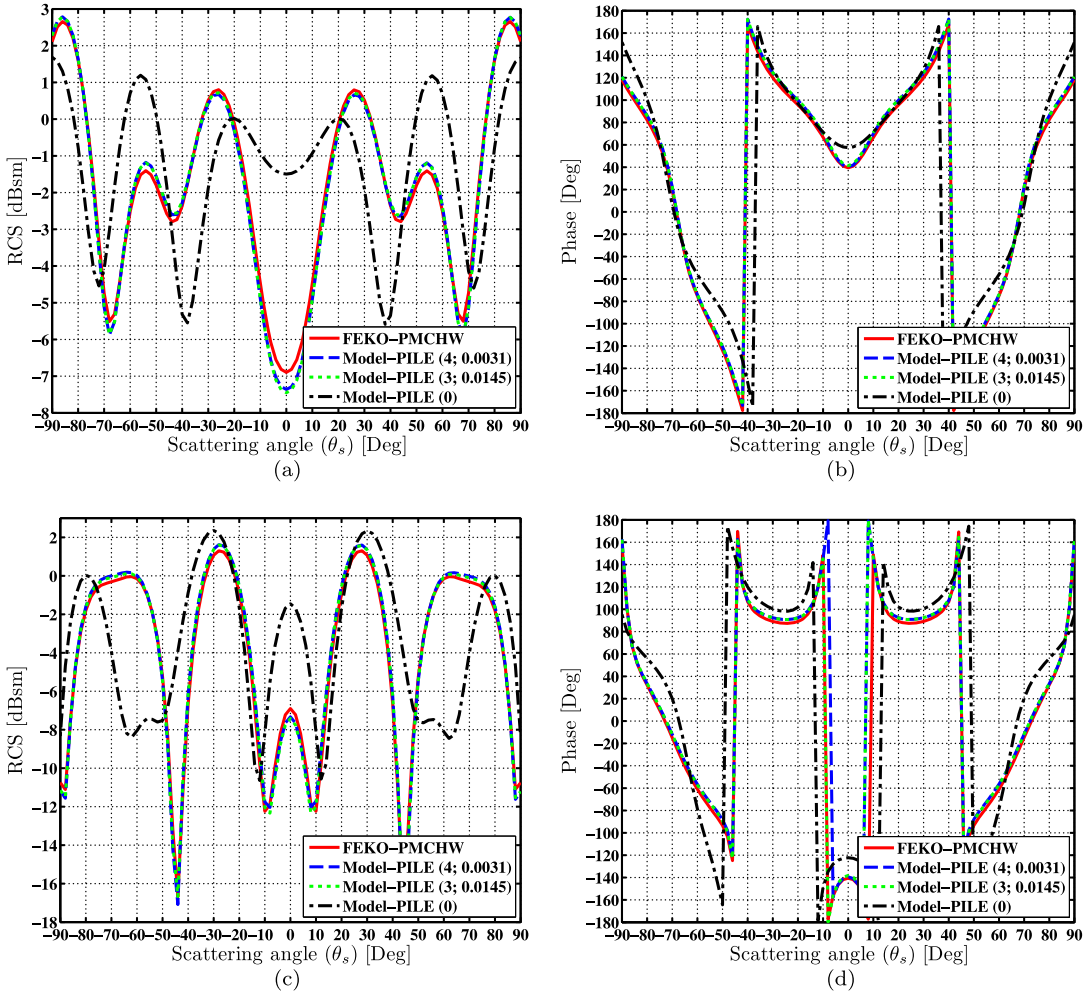

Fig. 3. Comparison between FEKO software and PILE-based model results on the copolarized bistatic RCS as well as on the phase of the scattered electric field of a structure consisting of two nested dielectric spheres with respect to scattering angle θ_s ($\phi_s = 0°$) for an incident plane wave frequency $f = 300$ MHz and direction $\hat{\mathbf{k}}_i(\theta_i = 0°, \phi_i = 0°)$. The interior sphere of relative permittivity $\epsilon_{\text{in}}^r = 2 - j8$ and radius $r_{\text{in}} = 0.5\lambda_1$ is embedded in an exterior sphere with relative permittivity $\epsilon_{\text{ex}}^r = 2 - j0.1$ and radius $r_{\text{ex}} = \lambda_1$. (a) VV polarization, (b) VV polarization, (c) HH polarization, and (d) HH polarization.

In Fig. 4, we plot the bistatic RCS of the structure $\mathcal{S}_2$ as a function of the angle θ_s for all of the polarization channels (VV, VH, HV, and HH). For this configuration, the curves indicate good agrement between the FEKO and PILE-based RCS for all of the polarization channels. The convergence of the PILE-based solution is obtained after $P_{\text{PILE}} = 3$ iterations with an error of 0.96% on the current densities associated with the exterior cylinder surface. The second-order PILE-based RCS values also represent a satisfactory result with an error of 5.03% on the current densities related to the exterior cylinder surface. Regarding the VV-polarized bistatic RCS values shown in Fig. 4(a), we observe a slight difference between the FEKO- and PILE-based levels in the angular range $\theta_s \in [-90°, -50°]$.

In Fig. 5, we show the bistatic RCS of the structure $\mathcal{S}_3$ as a function of the angle θ_s for all of the polarization channels. In this figure we can clearly observe very good agreement between FEKO and the PILE-based RCS values for all of the polarization channels. Furthermore, the PILE-based method convergence order is $P_{\text{PILE}} = 4$ with an error of 0.22% on the current densities associated with the exterior sphere surface. The curves also indicate that the PILE-based solution for a convergence order $p = 3$ provides a fairly good result on the full-polarized RCS with an error of 1.13%. As we mentioned earlier, the zeroth-order PILE-based solution accounts only for the scattering from the exterior sphere (it is as if the structure is composed only by the exterior object). This explains the symmetry of the curves associated with zeroth-order PILE-based copolarized RCS about the specular direction [Figs. 4(a) and 4(d)]. Given the interior cylinder orientation, this symmetry is immediately lost for higher-order PILE-based copolarized RCS. By analyzing the cross-polarized RCS values [Figs. 4(b) and 4(c)], we observe that the zeroth-order PILE-based RCS values are equal to zero (very low level corresponding to digital noise). This allows us to deduce that the higher-order cross-polarized RCS values of the structure $\mathcal{S}_3$ are mainly due to the contribution of the tilted interior cylinder. Therefore, the presence of the interior scatterer can be detected thanks to the cross-polarization channels.

According to the simulation results, we can conclude that the convergence order of the method PILE depends on the geometry of the scatterers, their dielectric parameters, and the thickness of the coating material.

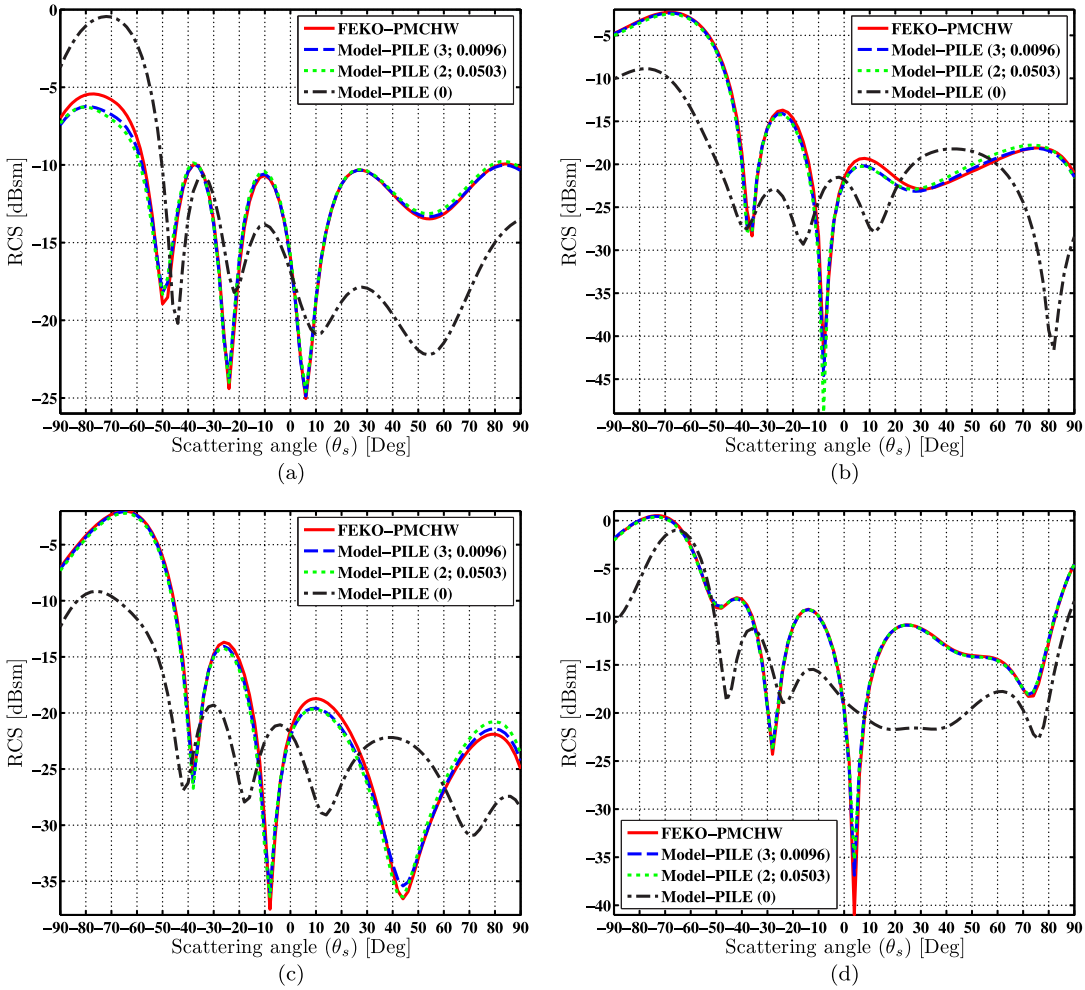

Fig. 4. Comparison between FEKO software and PILE-based model results on the full-polarized bistatic RCS of a structure consisting of two nested dielectric tilted cylinders with respect to scattering angle θ_s ($\phi_s = 0°$) for an incident plane wave frequency $f = 300$ MHz and direction $\hat{\mathbf{k}}_i(\theta_i = 0°, \phi_i = 0°)$. The interior cylinder of relative permittivity $\epsilon_{\text{in}}^r = 2 - j12$, radius $r_{\text{in}} = 0.5\lambda_1$, and length $h_{\text{in}} = 2\lambda_1$ is embedded in an exterior cylinder with relative permittivity $\epsilon_{\text{ex}}^r = 2 - j0.1$, radius $r_{\text{ex}} = 0.3\lambda_1$, and length $h_{\text{ex}} = 3\lambda_1$. (a) VV polarization, (b) VH polarization, (c) HV polarization, and (d) HH polarization.

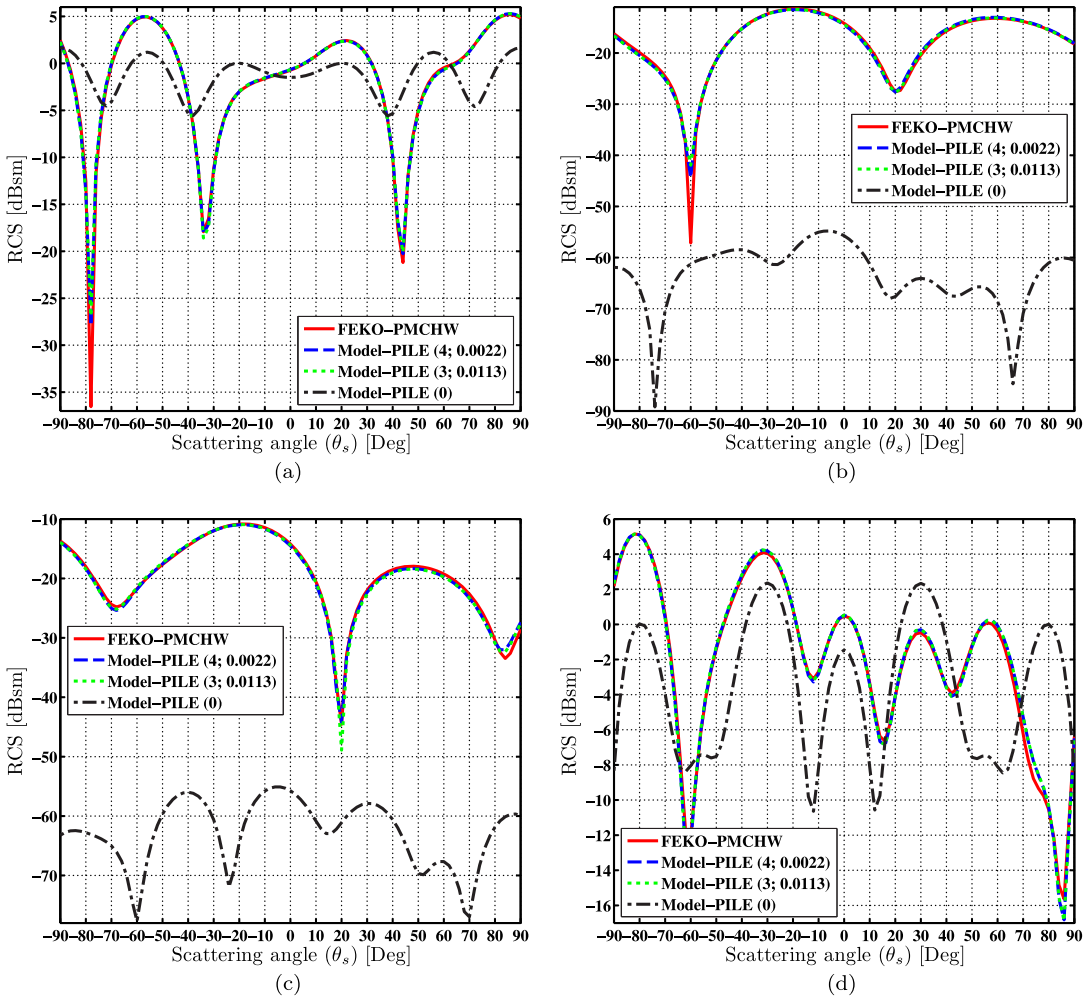

Fig. 5. Comparison between FEKO software and PILE-based model results on the full-polarized bistatic RCS of a structure consisting of a tilted PEC cylinder ($r_{\text{in}} = 0.2\lambda_1, h_{\text{in}} = 0.8\lambda_1$) embedded in a dielectric sphere ($\epsilon_{\text{ex}}^r = 2 - j0.1, r_{\text{ex}} = \lambda_1$), with respect to scattering angle θ_s ($\phi_s = 0°$) for an incident plane wave frequency $f = 300$ MHz and direction $\hat{\mathbf{k}}_i(\theta_i = 0°, \phi_i = 0°)$. (a) VV polarization, (b) VH polarization, (c) HV polarization, and (d) HH polarization.

7. CONCLUSION

In this paper, a PILE-based algorithm has been presented for the evaluation of EM scattering from 3D structures consisting of two nested homogeneous dielectric bodies with arbitrary shape. The problem was formulated in terms of PMCHW integral equations that are discretized by means of the Galerkin MoM with RWG basis functions. The resulting MoM matrix equation arising from these integral equations was iteratively solved by the PILE algorithm involving a significant reduction of computational cost in comparison to a direct inversion of the whole MoM impedance matrix. Some numerical results were presented to validate the algorithm implementation and illustrate the accuracy, the versatility, and the usefulness of the PILE-based approach on the analysis of the interaction of an EM wave with a complex 3D structure. As a guideline for future work, it is important to improve the performance of the PILE algorithm by accelerating the matrix-vector products in its iterative scheme. The principal idea is to compress the coupling matrices using the algebraic adaptive cross-approximation (ACA) algorithm [32], which reduces significantly the number of operations. Another idea is to hybridize the PILE approach with the current based physical optics (PO) asymptotic technique [2,16,31] in order to avoid the inversion of one of the self-impedance matrices.

ACKNOWLEDGMENTS

This work was supported by the French defence procurement agency DGA (Direction Générale de l'Armement) under ASTRID grant MCIED.

REFERENCES

1. E. Arvas and T. K. Sarkar, "RCS of two-dimensional structures consisting of both dielectrics and conductors of arbitrary cross section," IEEE Trans. Antennas Propag. **37**, 546–554 (1989).
2. C. Bourlier, N. Pinel, and G. Kubické, *Method of Moments for 2D Scattering Problems: Basic Concepts and Applications* (Wiley, 2013).
3. Y. M. Antar, A. A. Kishk, L. Shafai, and L. Allan, "Radar backscattering from partially coated targets with axial symmetry," IEEE Trans. Antennas Propag. **37**, 564–575 (1989).
4. T.-K. Wu and L. L. Tsai, "Scattering from arbitrarily-shaped lossy dielectric bodies of revolution," Radio Sci. **12**, 709–718 (1977).
5. K. Umashankar, A. Taflove, and S. M. Rao, "Electromagnetic scattering by arbitrary shaped three-dimensional homogeneous lossy dielectric objects," IEEE Trans. Antennas Propag. **34**, 758–766 (1986).

6. X. C. Nie, L. W. Li, N. Yuan, T. S. Yeo, and Y. B. Gan, "A fast analysis of electromagnetic scattering by arbitrarily shaped homogeneous dielectric objects," Microwave Opt. Technol. Lett. **38**, 30–35 (2003).
7. A. M. Kern and O. J. Martin, "Surface integral formulation for 3D simulations of plasmonic and high permittivity nanostructures," J. Opt. Soc. Am. A **26**, 732–740 (2009).
8. X. Q. Sheng, J.-M. Jin, J. Song, W. C. Chew, and C.-C. Lu, "Solution of combined-field integral equation using multilevel fast multipole algorithm for scattering by homogeneous bodies," IEEE Trans. Antennas Propag. **46**, 1718–1726 (1998).
9. R. E. Hodges and Y. Rahmat-Samii, "The evaluation of MFIE integrals with the use of vector triangle basis functions," Microwave Opt. Technol. Lett. **14**, 9–14 (1997).
10. S. M. Rao, D. Wilton, and A. W. Glisson, "Electromagnetic scattering by surfaces of arbitrary shape," IEEE Trans. Antennas Propag. **30**, 409–418 (1982).
11. J. M. Rius, E. Ubeda, and J. Parrón, "On the testing of the magnetic field integral equation with RWG basis functions in method of moments," IEEE Trans. Antennas Propag. **49**, 1550–1553 (2001).
12. E. Ubeda and J. M. Rius, "MFIE MoM-formulation with curl-conforming basis functions and accurate kernel integration in the analysis of perfectly conducting sharp-edged objects," Microwave Opt. Technol. Lett. **44**, 354–358 (2005).
13. O. Ergul and L. Gurel, "The use of curl-conforming basis functions for the magnetic-field integral equation," IEEE Trans. Antennas Propag. **54**, 1917–1926 (2006).
14. E. Ubeda and J. M. Rius, "Novel monopolar MFIE MoM-discretization for the scattering analysis of small objects," IEEE Trans. Antennas Propag. **54**, 50–57 (2006).
15. M. Kouali, G. Kubické, and C. Bourlier, "Extended propagation-inside-layer expansion method combined with the forward-backward method to study the scattering from an object above a rough surface," Opt. Lett. **37**, 2985–2987 (2012).
16. M. Kouali, G. Kubické, and C. Bourlier, "Electromagnetic interactions analysis between two 3-D scatterers using the E-PILE method combined with the PO approximation," Prog. Electromagn. Res. B **58**, 123–138 (2014).
17. X.-C. Nie, N. Yuan, L.-W. Li, Y.-B. Gan, and T. S. Yeo, "A fast volume-surface integral equation solver for scattering from composite conducting-dielectric objects," IEEE Trans. Antennas Propag. **53**, 818–824 (2005).
18. S. He, Z.-P. Nie, and J. Hu, "Numerical solution of scattering from thin dielectric-coated conductors based on TDS approximation and EM boundary conditions," Prog. Electromagn. Res. **93**, 339–354 (2009).
19. S. M. Rao, C.-C. Cha, R. L. Cravey, and D. L. Wilkes, "Electromagnetic scattering from arbitrary shaped conducting bodies coated with lossy materials of arbitrary thickness," IEEE Trans. Antennas Propag. **39**, 627–631 (1991).
20. W. C. Chew, M. S. Tong, and B. Hu, *Integral Equation Methods for Electromagnetic and Elastic Waves* (Morgan & Claypool, 2008).
21. L. Tsang, J. A. Kong, K.-H. Ding, and C. O. Ao, *Scattering of Electromagnetic Waves, Numerical Simulations* (Wiley, 2004), Vol. **25**.
22. W. C. Gibson, *The Method of Moments in Electromagnetics* (CRC Press, 2007).
23. L. Tsang, J. A. Kong, and K.-H. Ding, *Scattering of Electromagnetic Waves, Theories and Applications* (Wiley, 2004), Vol. **27**.
24. A. J. Poggio and E. K. Miller, *Integral Equation Solutions of Three-Dimensional Scattering Problems* (Oxford and Pergamon, 1973).
25. L. Medgyesi-Mitschang, J. Putnam, and M. Gedera, "Generalized method of moments for three-dimensional penetrable scatterers," J. Opt. Soc. Am. A **11**, 1383–1398 (1994).
26. B. H. Jung, T. Sarkar, and Y.-S. Chung, "A survey of various frequency domain integral equations for the analysis of scattering from three-dimensional dielectric objects," Prog. Electromagn. Res. **36**, 193–246 (2002).
27. P. Yla-Oijala and M. Taskinen, "Calculation of CFIE impedance matrix elements with RWG and n×RWG functions," IEEE Trans. Antennas Propag. **51**, 1837–1846 (2003).
28. M. M. Ney, "Method of moments as applied to electromagnetic problems," IEEE Trans. Microwave Theor. Tech. **33**, 972–980 (1985).
29. N. Déchamps, N. de Beaucoudrey, C. Bourlier, and S. Toutain, "Fast numerical method for electromagnetic scattering by rough layered interfaces: propagation-inside-layer expansion method," J. Opt. Soc. Am. A **23**, 359–369 (2006).
30. C. Bourlier, G. Kubické, and N. Déchamps, "Fast method to compute scattering by a buried object under a randomly rough surface: PILE combined with FB-SA," J. Opt. Soc. Am. A **25**, 891–902 (2008).
31. C. Bourlier, N. Pinel, and G. Kubické, "Propagation-inside-layer-expansion method combined with physical optics for scattering by coated cylinders, a rough layer, and an object below a rough surface," J. Opt. Soc. Am. A **30**, 1727–1737 (2013).
32. G. Kubické, C. Bourlier, S. Bellez, and H. Li, "A fast EPILE +FBSA method combined with adaptive cross approximation for the scattering from a target above a large ocean-like surface," Prog. Electromagn. Res. M **37**, 175–182 (2014).